Korean J. Chem. Eng., 37(10), 1732-1742 (2020)
DOI: 10.1007/s11814-020-0591-5

pISSN: 0256-1115
eISSN: 1975-7220

Effect of molecular weight of regenerated silk fibroin on silk-based spheres for drug delivery

Zengkai Wang*, Xiangming Li*, Yanhua Cui*, Kai Cheng*, Mingdong Dong, and Lei Liu*,†**

*School of Materials Science and Engineering and Institute for Advanced Materials, Jiangsu University, Zhenjiang, 212013, China
**Interdisciplinary Nanoscience Center (iNANO), Aarhus University, DK-8000 Aarhus C, Denmark
(*Received 14 March 2020 • Revised 14 May 2020 • Accepted 27 May 2020*)

Abstract−Silk fibroin presents a good advantage as a drug carrier for drug delivery, due to the excellent biocompatibility, biodegradability and tunable drug loading and release properties. In this work, we constructed silk spheres by phase separation of the regenerated silk fibroin (RSF) solutions with different MW and polyvinyl alcohol; and it was revealed that MW of RSF can affect the structure, size, surface potential and drug loading and release efficiency of silk spheres. Silk spheres prepared from high MW of RSF were found to load more macromolecular drug with negative charge compared to middle and low MW of RSF. However, for the positive charge and low MW drug, the silk spheres prepared from low MW of RSF could present a high loading efficiency compared to other carriers. Finally, a positive drug with low MW, streptomycin was encapsulated in silk spheres prepared from low MW of RSF, and displayed a long bactericidal and bacteriostatic effect compared to bared streptomycin solution. The results obtained provide guidelines for the modification and options of drug transport vehicles for more efficient drug delivery and utilization through a simple, rapidly constructed, applicable and low-cost drug carrier.

Keywords: Silk Fibroin, Encapsulation and Release, Release Kinetics, Streptomycin, Antibactericidal Material

INTRODUCTION

Silk fibroin (SF), a natural protein biopolymer extracted from the caterpillar *Bombxy mori*, presents excellent biocompatibility, outstanding mechanical stability, tunable degradability and natural self-assembly [1,2]. SF has been utilized and discussed extensively in biomedical research, such as a carrier for drug controlled release [3,4], tissue scaffolds [5-7] and enzyme immobilization [8,9], which is comparable to the other biopolymers, *i.e.*, peptide based material and liposomes [10-13]. The various structures were constructed from SF and used as biomaterials, such as micro- or nanoparticles, films, nanofibers and hydrogel [14-16]. Especially, silk micro- or nanoparticles have attracted significant attention and been widely used as the drug carriers in biomedical and pharmaceutical applications due to the high drug encapsulation efficiency without loss of drug activity, sustained release feature and tunable release kinetics [17,18].

To control the release of drug in silk-based carriers, many factors need to be considered, such as MW and charge of drug [19], the structure [20] and size [21] of drug carriers, sometimes the shape of carrier also affects the drug release profiles [22]. For instance, the size of drug carrier can adjust the drug loading and releasing [23-25]. Controlling the size of particles could enable the short- or long-term delivery of a drug [26,27], because the drug could release fast in the small carrier, due to the short diffusion distance. The molecular weight (MW) of the polymer is also a key factor to the sizes, structures and mechanical properties and biodegradability of constructed materials [28,29], which could be significant in drug delivery. It was reported that the loading and release of a drug can be modulated and controlled by changing the MW of silk carriers. For instance, Mitropoulos et al. fabricated different size particles by microfluidics and using regenerated silk fibroin (RSF) with different MW to display distinct release features [21]. It is also found that the biological properties of a drug carrier could be significantly affected by modulating MW of SF carrier, *e.g.*, the cell viability and the macrophage activation [30]. However, in most cases, a single MW drug carrier was used for different drugs without considering the drug properties and adaptability between the drug and drug carriers [3,31-33]. Therefore, a rational design of delivery system should be considered to load and release drug according to the different specific requirements, and general evaluation of release profiles of drug carriers according to different properties of drug molecule could be necessary.

Many methods have been developed for preparing silk particles, such as emulsification diffusion [34], silk/PVA blend film [3], spray-drying [35], microfluidics [36], salting out [37] and laminar jet break-up [38]. Each method has advantages and disadvantages; the instrumental-based methods (laminar jet, microfluidics) are easy to scale up by using industrial machines; however, these methods require expensive instruments and need operational expertise. Chemical-based methods, such as desolvation [39], salting out, emulsification diffusion and polymer blending, have mild processing conditions and simple operation. However, desolvation and emulsification diffusion are not suitable for drug delivery applications because

†To whom correspondence should be addressed.
E-mail: liul@ujs.edu.cn

of the use of organic solvents. The polymer blending method (*i.e.*, SF/polyethylene glycol (PEG), SF/polyvinyl alcohol (PVA)) has the advantages of simple operation, mild condition, no organic solvent and controllable crystallinity and particle size [3,20,40]. PVA is non-toxic and water-soluble polymer which has FDA approval for clinical uses in humans [41,42]. The effect of SF/PVA blend on physicochemical property of SF has been studied; it was found that the concentration and MW of PVA and ratio between PVA and SF have an effect on the morphology, size and the secondary structure of SF particles [3,21,43]. We chose the RSF/PVA blending method, which is a relatively simple method without using non-toxic solvents, and useful to keep the bioactivity of encapsulated drug molecules and mild preparation conditions to construct the drug carrier [44].

In this work, we explored the effect of different MW of RSF on the encapsulation and release of different molecules as the model and achieved an effective utilization and optimum for different drugs. The SF spheres prepared from high MW of RSF could load more macromolecular drugs with negative charge compared to middle and low MW of RSF. However, the spheres prepared from low MW of RSF could show high encapsulation efficiency compared to other carriers for the positive charge and low MW drug. Finally, streptomycin (STM) as a drug, for instance, was utilized to investigate the slow-release sterilization behaviors of STM encapsulated SF spheres.

MATERIALS AND METHODS

1. Materials

Cocoons of *Bombyx mori* silk were supplied by Sericulture factory (Yang Zhong, Jiangsu province, China). Poly vinyl alcohol (PVA, average mol wt, 30 k-70 kDa), model drugs Fluorescein isothiocyanate conjugated bovine serum albumin (FITC-BSA, 66 kDa), fluorescein isothiocyanate conjugated dextran (FITC-Dextran, 10 kDa), Rhodamine B (RhB, 479 Da) were purchased from Sigma-Aldrich.

2. Silk Fibroin Purification

Silkworm cocoons were boiled in 0.02 M Na_2CO_3 solution with time control (15 min, 30 min, 45 min and 60 min, respectively), the temperature used for Na_2CO_3 solution was about 100 °C, and then rinsing with distilled water for three times. After air drying overnight, degummed silk fibroin was dissolved in 9.3 M lithium bromide (LiBr) solution at 60 °C for 3 hours; the dialysis of this solution against deionized water [1] (dialysis tube, MWCO 3.5 kDa, Union Carbide) ultimately generates silk fibroin solution with different average molecular weight. These samples are hereafter referred to as 15 min, 30 min, 45 min and 60 min according to boiling time (15 min, 30 min, 45 min and 60 min).

3. Measurement of Regenerated Silk Fibroin Average Molecular Weight

The average molecular weight of RSF was performed with sodium dodecyl sulfate polyacrylamide gel electrophoresis (SDS-PAGE). All samples were mixed with 5X SDS-PAGE loading buffer, then heated at 95 °C for 5 min, and the denatured samples were loaded into a 4-20% gradient gel (EZBiolab, Cat. #: GSH2001-420T), running at 150 V for 50 min and stained with an Easy Stain Coomassie Blue Kit (Invitrogen, Carlsbad, CA). The molecular weight distribution was quantified by densiometric measurement along the gel according to molecular weight markers (Image J, NIH, MD).

4. Preparation of SF Spheres

RSF and PVA aqueous solutions were prepared at the same concentration of 3% w/v, respectively. Subsequently, four RSF/PVA blending solutions were designed with the weight ratio of RSF to PVA were 2/1, 1/1, 1/2 and 1/4 for concentration of 3% w/v, then diluted solutions of RSF and PVA solution were blended with a weight ratio of RSF to PVA were 2/1, 1/1, 1/2 and 1/4 at concentrations of 1% w/v. The blending solution was vortexed in centrifuge tube for 20 s at 1,500 rpm/min prior to dry. To keep the similar drying rates, the mixed solution with different concentration and the same weight ratio was transferred into open polystyrene petri dishes with same size. All the samples in the dishes were dried to film at 37 °C overnight, before further dried at 60 °C for 30 min. All the films were dissolved in ultrapure water with gentle shaking (150 r/min) at 37 °C. The SF spheres were collected by centrifuging at 10,000 r/min for 10 min. The particles were rinsed twice with deionized water.

5. Characterization

5-1. Fourier Transform Infrared Spectroscopy (FTIR)

FTIR analysis of SF particles was performed by a Thermo Scientific™ Nicolet™ iS50 FTIR Spectrometer (Thermo Scientific, USA) equipped with a diamond attenuated total reflectance (ATR) mode. Each sample was scanned 64 times from 400 to 4,000 cm^{-1} with a resolution of 4 cm^{-1}. The main crystal structures of SF were silk I (random coils, alpha-helices and turns) and silk II (β-sheets); these conformations have different absorbance band in FTIR. The fractions of secondary structural components were evaluated using Fourier self-deconvolution (FSD) of the infrared absorbance spectra, and then used to determine the difference of RSF spheres prepared from RSF with different molecular weight. FSD was analyzed by the Omnic 8 software.

5-2. Scanning Electron Microscopy (SEM)

50 μL of the SF particles suspensions was directly dropped on the Si substrate mounted on an SEM sample stub. The samples were dried overnight and then sputtered with platinum. The morphology of the SF particles was characterized using a JSM-7800F Thermal Field Emission SEM (JEOL, Japan).

5-3. Particle Size Distribution and Zeta Potential

The size distribution of the SF particles were determined using a Nano ZS90 laser particle size analyzer (Malvern, England) as previously described [31]. Briefly, silk spheres suspension (10 μg/mL) was added to a cuvette, which was loaded in ZS90 at 25 °C. The Zeta potential of the SF spheres was also measured using the same equipment at 25 °C in deionized water at neutral.

5-4. Drug Loading in Silk Particles

FITC-BSA, FITC-Dex and RhB were used as the model drugs. Each drug stock solution was prepared with a concentration of 5 mg/mL in phosphate buffered saline (PBS) buffer, pH 7.4 and stored at −20 °C. The drug solutions were mixed with silk solution at a weight ratio of 1 (drug): 200 (silk) for 10 min prior to mixing with PVA solution and generating a blend film. The final blend solution was used to generate particles as described above but without vortex treatment. The loaded spheres were rinsed three times with deionized water. The supernatants collected from the centrifugation and wash steps were subjected to fluorescence measurement

(excitation wavelength (E_x): 493 nm and an emission (E_m): 520 nm for FITC-BSA and FITC-dextran, and E_x: 550 nm, E_m: 580 nm for RhB) (F4500, Hitachi), to determine the drug residual amount in solution and the drug loading in SF spheres. The drug quantification was calculated based on a standard calibration curve obtained at the same condition (R^2>0.99).

Each sample was performed in triplicate. Encapsulation and loading efficiency were calculated using Eqs. (1) and (2), respectively:

$$\text{Encapsulation efficiency (w/w\%)} = \frac{\text{amount of drug in silk particles}}{\text{total drug initially added}} \times 100 \quad (1)$$

$$\text{Loading (w/w\%)} = \frac{\text{amount of drug in silk particles}}{\text{amount of silk particles}} \times 100 \quad (2)$$

5-5. Confocal Laser Scanning Microscopy

The distribution of model drug molecules in SF spheres was determined by confocal laser scanning microscopy. The drug-loaded SF spheres were prepared as described above and then re-suspended in deionized water. The sample was imaged using a Leica TCS SP5 II microscope (Leica, Germany) at an excitation wavelength (E_x) of 493 nm and an emission (E_m) of 520 nm for FITC-BSA and FITC-dextran, and E_x: 550 nm, E_m: 580 nm for RhB.

5-6. Drug Release from the Silk Spheres

Lyophilized SF particles with loaded drug were suspended in 1 mL PBS (pH 7.4) with constant shaking (150 r/min) at 37 °C. At 1, 2, 4, 12, 24, 48, 96, 144, and 196 h, the particles suspensions were centrifuged (10,000 r/min, 5 min) and replaced with fresh PBS (pH 7.4). The supernatant was collected for analysis as described above.

5-7. Release Kinetics

The rate and mechanism of the release of drugs from SF particles were discussed by fitting the date with zero-order equation [45]:

$$Q = k_0 t$$

first-order equation [45]:

$$\ln(100 - Q) = \ln 100 - k_1 t$$

where Q is the amount of drug released at time t, k_0 and k_1 are the release rate constant.

The Korsmeyer-Peppas equation [46]:

$$\frac{M_t}{M_\infty} = kt^n$$

where the M_t/M_∞ is the fractional release of the drug at time t, k is a constant, and *n* is the diffusional exponent.

6. Slow-release Sterilization Performance of Streptomycin-loaded SF Spheres

STM was encapsulated in silk spheres as described method of model drugs. STM-loaded SF spheres and silk spheres without STM were suspended in 1 mL of PBS, respectively. Then, 10 μL of bacterial suspensions (*E. coil.* 2×10^7 cfu/mL) was added into above solutions to achieve a bacterial concentration of 2×10^5 cfu/mL. 1 h later, 2 μL of the suspension was added into 2 mL of PBS to dilute about 1,000-fold, and then 100 μL of diluted sample was spread on an LB agar culture plate and cultured at 37 °C for 16 h. As control groups, 0 μg, 10 μg and 110 μg of STM were added into 1 mL of PBS solution, respectively. 10 μL of fresh bacterial suspensions (2×10^7 cfu/mL) were added into each sample per 12 hours, and 2 μL of sample from mixture were collected and spread on an LB agar culture plate as described above. The concentration of STM was measured according to the method as described in previous studies [47].

RESULTS AND DISCUSSION

1. Preparation of Regenerated Silk Fibroin with Different Molecular Weight

The RSF solution was obtained through degumming, dissolving and dialysis process. SDS-PAGE was used to isolate the protein with different MW because the electrophoretic mobility was correlated to protein size (MW) and folding [30]. All the samples were heated to 95 °C for 5 min to fully denature the protein. SDS-PAGE showed that each sample had as a smear that appeared down the gel with the degumming time increased (Fig. 1(a)), and suggest-

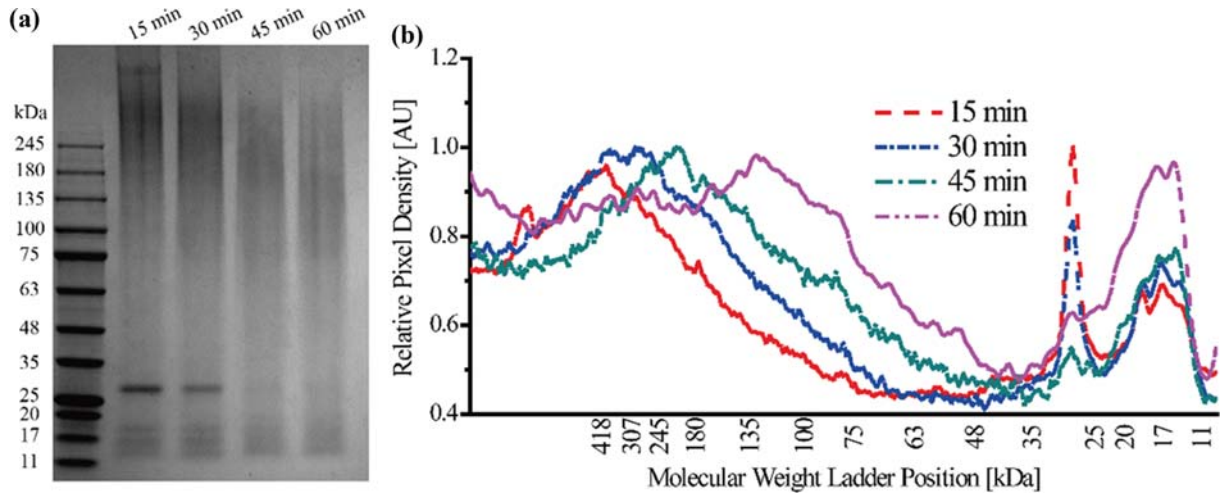

Fig. 1. Molecular weight analysis of RSF solutions. (a) SDS-PAGE of different samples; (b) densiometric analysis of regenerated silk fibroin protein distribution according to the gel.

ing that the RSF was degraded into lower MW fragments. We utilized the densiometric analysis to examine the MW distribution of RSF prepared form different boiling time (15 min, 30 min, 45 min and 60 min), which displayed distinct wide distributions of MW according to the molecular weight markers (around 400 kDa, 290 kDa, 190 kDa and 120 kDa) (Fig. 1(b)). Furthermore, both 15 min sample and 30 min sample have a visible peak around 27 kDa, while other two samples only displayed a small peak accordingly. All the samples presented a broad peak around 17 kDa. The results above implied that the MW distribution of RSF solution was able to be modulated generally by controlling boiling time.

2. SF Spheres Preparation and Characterization

We constructed SF spheres with a uniform size distribution via the phase separation between the prepared RSF with different MW and PVA under relative mild condition. PVA was employed in the reaction as an emulsifier, and the PVA molecular could give SF spheres independent space to assemble and simultaneously prevent aggregation of spheres. The SF spheres were produced via self-assembly of regenerated silk fibroin (RSF) under gentle condition. When the RSF solution and polyvinyl alcohol (PVA) solution were blended and subsequently cast into film under weight ratio of RSF and PVA constant at 1/4, the blend solution was macroscopically uniform. Due to the RSF and PVA being immiscible, the microscopic phase separation between the RSF and the PVA occurred spontaneously in the blend film and the phase separation was dependent on the ratio between RSF and PVA [48,49]. The solution of RSF and PVA was mixed to dry to prepare the blend film, and subsequently the silk particles could be obtained by removing PVA and water. Drying the blend solution into a film, the microspheres and nanospheres were observed in the RSF/PVA blend film. Drying the blend solution into film was an essential step for formation of stable water-insoluble RSF spheres, because β-sheet structure formed by the self-assembly of RSF could stabilize the structure of SF spheres. The concentration and weight ratio of RSF and PVA do affect the structure of silk-based particles. Therefore, systematic explorations were performed. RSF and PVA with two concentrations of 3% w/v and 1% w/v were blended at different weight ratio of RSF to PVA (2/1, 1/1, 1/2 and 1/4), respectively, and then cast into films. It was found that all the dried RSF/PVA films prepared from 30 min (290 kDa), 45 min (190 kDa) and 60 min (120 kDa) displayed good solubility and finally could be constructed to form silk particles, expect for the ones from 15 min (400 kDa) that form many sheets in solution, because the large MW originating from 15 min (400 kDa) sample could easily form β-sheet in the process. Furthermore, it was proved that low concentration such as 1% w/v led to a low yield of spheres for the RSF/PVA films pre-

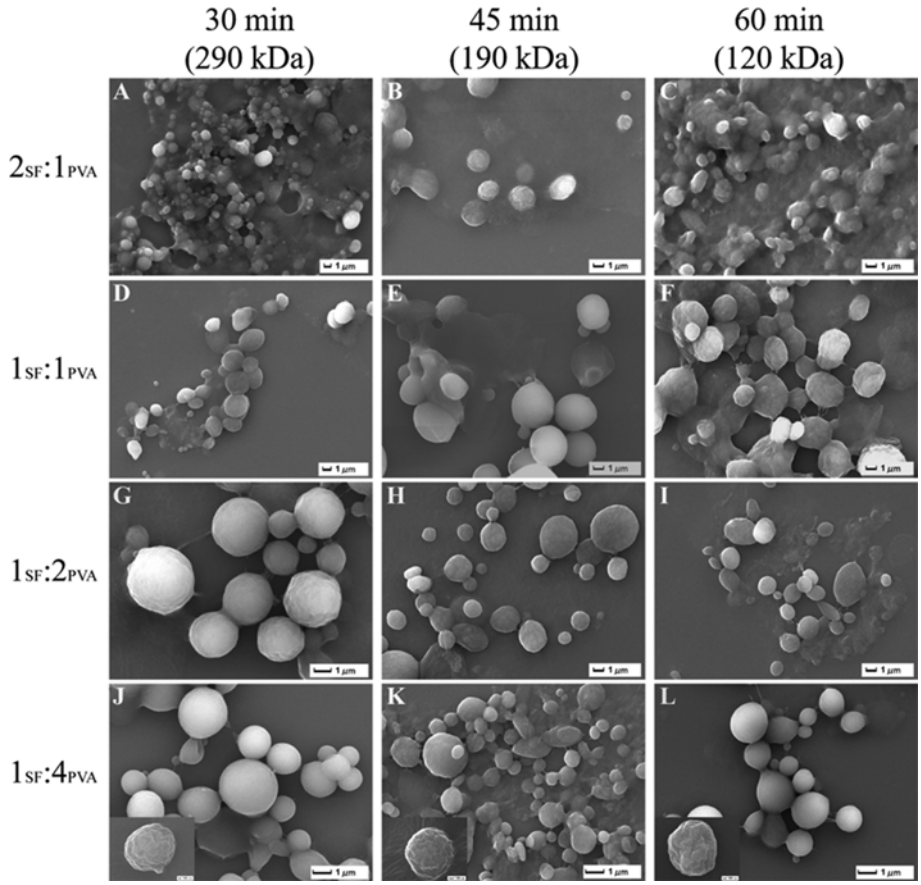

Fig. 2. The SEM images of SF particles with size control by modulating weight ratio of RSF and PVA. The concentration of both RSF and PVA was 3% w/v (A-C, D-F, G-I, J-L). The morphologies of SF particles prepared from different MW by boiling time control at the weight ratio of 2/1, 1/1, 1/2, and 1/4 between RSF to PVA, respectively. The inset of J, K and L showed a detailed surface structure of individual SF particle (scale bar, 100 nm).

pared from 30 min (290 kDa), 45 min (190 kDa) and 60 min (120 kDa) RSF solution at all weight ratio between RSF and PVA above. Therefore, we selected and characterized the high yield samples prepared from the concentration of 3% w/v for further application in drug delivery.

SF particles of various weight ratio of RSF and PVA at 3% w/v were characterized (Fig. 2). Silk particles could retain a spherical shape and could be readily spun down and resuspended. PVA was employed in the reaction as an emulsifier, and the PVA molecular could give SF spheres independent space to assemble and simultaneously prevent aggregation of spheres. The SF spheres were produced via self-assembly of RSF under gentle condition. PVA had significant influence on the formation of silk particles and surface morphology. The SF particles prepared RSF/PVA blends films with weight ratio of 2/1 were surrounded by membrane-like structure (Fig. 2A-C); it might be that PVA content was too small to provide enough space for self-assembly of SF, and resulting in a part of the SF failing to form particles, which caused the SF particles to aggregate and stick together. Compared with Fig. 2A and Fig. 2C, the pellet-forming capacity of SF spheres prepared from higher MW of RSF was higher than that of SF spheres prepared from lower MW of RSF. When RSF/PVA blend films with weight ratio of 1/1, the formed SF particles were irregular spherical shape, with an decrease in the MW of RSF; a circular disk SF particles was observed (Fig. 2F), which might be due to the unstable structure of SF spheres prepared with low MW and easy to deform under external force. With the increase of PVA, for example, the RSF/PVA blend films with weight ratio of 1/2 and 1/4, the blend films could quickly dissolve in water to form a homogeneous suspension within 15 min. As can be seen in Fig. 2G-L, the SF particles contained micro- and nanoparticles with rough surfaces; these SF particles presented a regular spherical shape, and all the particles were washed twice after blend film dissolution, due to more complete removal of the PVA. The formed SF particles had a narrower size distribution (see Table 2) compared to the samples prepared from the RSF/PVA blend films with weight ratio of 2/1 and 1/1 (Fig. 2A-F). The observed SF particle sizes were smaller than that of DLS, which probably resulted from the dehydration during preparation process of SEM samples and resulted in the shrinkage of the SF particles. Especially, the SF spheres exhibited a wrinkled surface (Fig. 2J, K, L inset), which was the feature of silk particles as prepared.

To characterize the secondary structure of SF based spheres, FTIR was performed on RSF solution and lyophilized SF spheres ($1_{SF}/4_{PVA}$) prepared from the directly dissolved RSF/PVA blend films. The secondary structure of silk fibroin mainly included silk I (random coils and/or α-helix) and silk II (β-sheet). In FTIR spectra, the position of these absorption bands was attributed to the secondary conformation of silk fibroin; 1,653 cm^{-1} (random coil) and 1,627 cm^{-1} (β-sheet) for amide I, 1,545 cm^{-1} (random coil) and 1,520 cm^{-1} (β-sheet) for amide II, and 1,236 cm^{-1} (random coil) and 1,243 cm^{-1} (β-sheet) for amide III [50,51]. In this case, FTIR spectra of the RSF aqueous solution and the particles were tested in Fig. 3(a) and 3(b). The peaks at 1,654, 1,550 and 1,247 cm^{-1} represented the typical random coils/extended chains structure (Fig. 3(a)). Four samples showed a similar FTIR spectrum indicating the secondary structure remained the same in RSF solution. In case of SF particles, the 1,635 cm^{-1} (60 min (120 kDa)), 1,623 cm^{-1} (45 min (190 kDa)) and 1,622 cm^{-1} (30 min (290 kDa)) for amide I were observed, which represented β-sheet secondary structure.

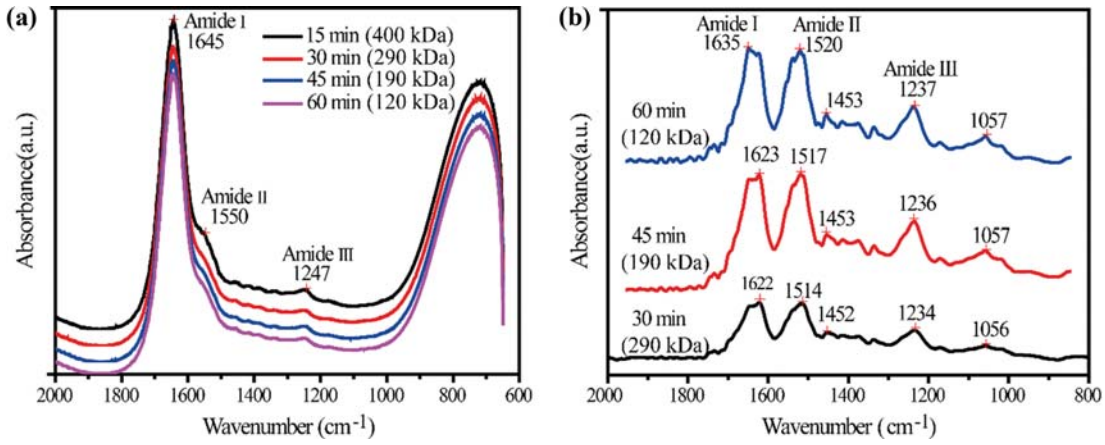

Fig. 3. FTIR spectra of (a) RSF solution prepared from different MW according to different boiling time and (b) SF spheres prepared by mixing with PVA solution with the concentration of 3% w/v and weight ratio $1_{SF}/4_{PVA}$.

Table 1. Secondary conformation content in SF spheres prepared from RSF/PVA films

Sample	β-Sheet content (%)	Random coils content (%)	α-Helices content (%)	Turns content (%)
30 min (290 kDa)	48.0±4.1	21.0±2.7	16.1±2.8	14.3±2.4
45 min (190 kDa)	41.0±3.5	20.9±3.2	15.6±2.2	14.3±1.9
60 min (120 kDa)	35.5±3.1	29.9±2.2	10.0±1.7	15.0±1.2

Table 2. Average diameter, polydispersity (PDI) and Zeta potential of SF spheres

RSF sample	RSF/PVA concentration (wt%) and weight ratio	Average diameters (nm)	PDI (a.u.)	Zeta potential (mV)
30 min (290 kDa)	3%, 1 : 4	1,567±308	0.146	−6.24
45 min (190 kDa)	3%, 1 : 4	761±105	0.353	−7.80
60 min (120 kDa)	3%, 1 : 4	1,356±283	0.123	−6.84

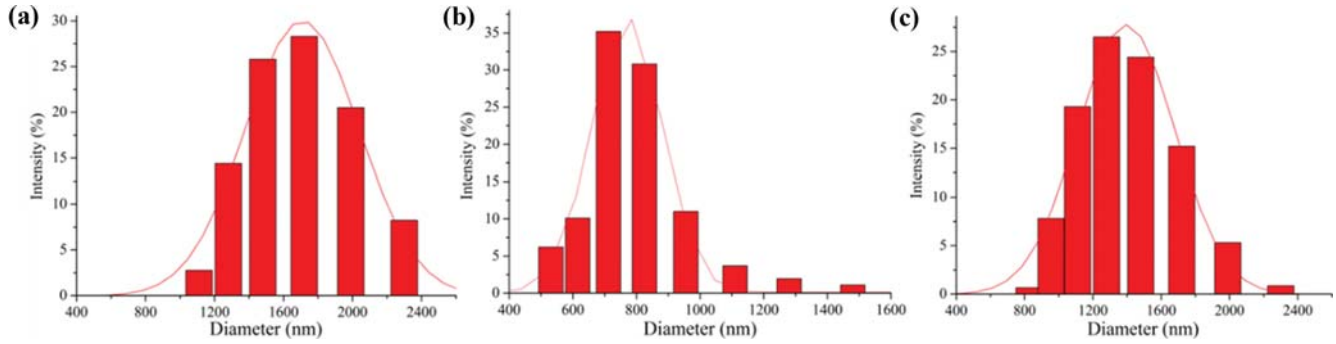

Fig. 4. The size distribution of SF spheres prepared form different MW of RSF. (a) 30 min (290 kDa); (b) 45 min (190 kDa); (c) 60 min (120 kDa).

The particles constructed by different MW SF presented slight shifts of vibration band. The SF spheres prepared from 30 min (290 kDa) had less β-sheet content compared to the one from 45 min (190 kDa) and 60 min (120 kDa) by the analysis of secondary structure (Table 1) [52]. The content of β-sheet of SF decreased with the decrease of RSF MW, which led to the decrement of the overall crystallinity. Random coil occupied less in the secondary structure of SF mainly due to the length of molecular chain of silk decreasing and restricting the bending and folding of the molecular chain and the formation of intramolecular hydrogen bond and forming the intermolecular β-sheet.

3. Particle Size and Zeta Potential

Particle size and Zeta potential of carriers are the key factors to affect the drug loading and releasing. The size of SF spheres prepared from RSF/PVA blend films varied from several hundred nanometers to a few micrometers due to the difference of MW of RSF (Table 2). For instance, as shown in Fig. 4, the average size of prepared spheres was 1,567 nm for 30 min (290 kDa), 761 nm for 45 min (190 kDa) and 1,356 nm for 60 min (120 kDa). The MW of RSF decreased with boiling time, and the length of the chain decreased with decrease of MW. At the same concentration of RSF solution, the viscosity of solution of RSF also decreased with the decrease of MW, and the mobility of lower MW of RSF faster than that of higher MW of RSF. According to the microscopic images in the literature [3], the RSF solution, which formed the droplets in the blend solution, dispersed in the surrounding PVA solution, which was analogous to W/O emulsion. In addition, we found that the RSF/PVA blend solution from 60 min (120 kDa) (lower MW of RSF) took longer to dry the blend solution into a film than that of RSF/PVA blend solution from 30 min (290 kDa) and 45 min (190 kDa) (higher MW of RSF) at the same concentration and other experiment conditions, the RSF/PVA blend solution from 60 min (120 kDa) was less stable than RSF/PVA blend solution from 30 min (290 kDa) and 45 min (190 kDa). These RSF droplets in RSF (60 min)/PVA blend solution might incorporate into bigger droplets due to lower viscosity and greater mobility of RSF (60 min), resulting in an increase in the size of SF spheres.

The zeta potential of SF spheres is in the range of −6 to −8 mV (Table 2), which was negative charge on the surface of spheres. The lower zeta potential might lead to agglomeration and poor dispersion of drug-loaded SF particles. The stability of SF spheres suspension was good after being stored for a few days, as observed during sample storage at 4 °C. Precipitation was observed after being stored for over a week; they could be readily resuspended through shaking or sonicating for a few seconds.

For the zeta potential values, it was found that the zeta potential of SF spheres was related to its concentration; it might due to the mechanism of electrophoretic light scattering used in measuring zeta potential of colloidal solution, because particles with a high concentration could reduce the scattered light and the laser beam become attenuated [53]. For the measured zeta potential in Table 2, the concentration of SF spheres was 10 μg/mL. The zeta potential could be decreased by −27 mV by increasing the concentration to 100 μg/mL. When the concentration was further increased to 300 μg/mL, the zeta potential instead increased to around −8 mV. Self-assembly of different chains length and conformation of different MW of RSF were different, which might be similar to the effect of pH on secondary structures and zeta potentials of SF particles [37].

4. Drug Loading and Release

Drug loading and encapsulation efficiency are supposed to be closely related to the molecular weight of carriers, the conformation of the biopolymer and polymer-drug interactions [54]. To test the drug loading and release in SF spheres composed of RSF with different MW, three molecules as the models were used to be encapsulated in SF spheres, FITC-BSA (negative charge, 66 kDa),

FITC-dextran (neutral, 10 kDa) and RhB (positive charge, 479 Da). The three molecules displayed different hydrophobicity, (RhB (log P: 1.95)>FITC-BSA (log P: 0.1-0.5 [55,56])>FITC-Dex (log P: −7.2)). The different drug loading and release efficiency in SF spheres were determined for these three drug model molecules. Generally, SF spheres prefer to encapsulate the positive charge molecule with low MW, such as RhB, the encapsulation efficiency of which was determined to be about 44% for 30 min (290 kDa), 74% for 45 min (190 kDa) and 68% for 60 min (120 kDa) sample. The SF spheres presented the lowest encapsulation efficiency for Dex, only 3%-4% obtained, and for BSA 35%- 25% obtained in different SF spheres with different MW. Both FITC-BSA and silk were proteins and have a similar structure, including hydrophobic and hydrophilic parts; the FITC-BSA interacted with silk due to the hydrophobic interactions and electrostatic binding; interactions of higher MW of silk with FITC-BSA were stronger than other lower MW samples during silk sphere preparation, which decreased the encapsulation efficiency dramatically. Because, the FITC-Dex was neutral and hydrophilic, and encapsulation efficiency went up with increased boiling time, behaving contrarily to FITC-BSA. But tiny amount of FITC-Dextran was loaded in the silk spheres in all samples, probably because its hydrophilic property, electrical neutral and diverse structure, although its molecular weight was outstandingly lower than that of FITC-BSA. In the slow-release system of silk fibroin materials, drug molecules could be distributed in the amorphous area and might also exist in between the β-folded lamellae of the crystalline region; however, the content of drug molecules in the crystal region was relatively small, because the crystalline region was a stable β-sheet structure and the arrangement was relatively tight. In addition, due to the swelling of amorphous structure being easy to occur in aqueous solution [57], when water molecules penetrated into the matrix and loosened the skeleton, the drug molecules in the non-crystalline region were easy to dissolve and release. Based on the result of Table 1, with the decrease of MW of SF the β-sheets content of SF spheres prepared from three MW decreased, and the content of amorphous structure increased. The repetitive part (pI=3.8) of heavy chain consists of long hydrophobic domains with short intervening hydrophilic spacers with negative charges [37]. The stability of high content of β-sheets was not conducive to the drug load. In contrast, high content of amorphous structure and lower β-sheets content have a greater degree of swelling in water, while the MW of RhB was lower, which was much easier to diffuse out of the silk particles. Therefore, the SF spheres prepared from 45 min (190 kDa) had the relative highest loading efficiency.

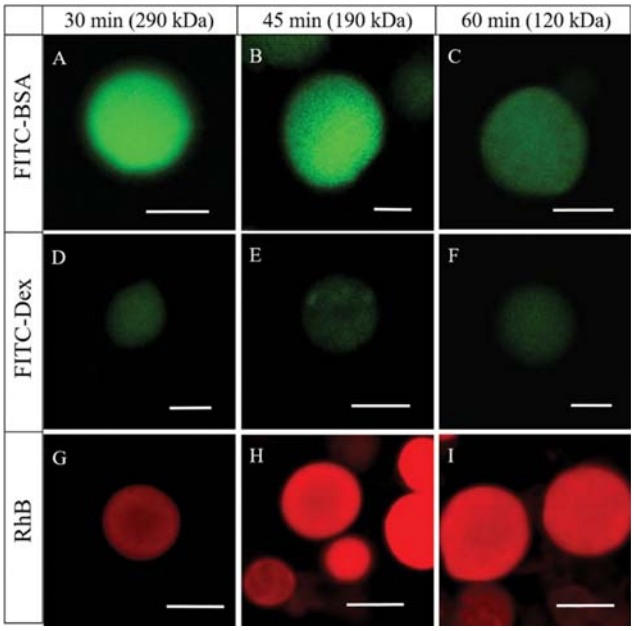

Fig. 5. Drug loading and distribution in SF spheres. Confocal images of the SF spheres prepared from different MW, loading FITC-BSA (A-C), FITC-Dex (D-F), and RhB (G-I), respectively. Scale bar, 4 μm.

Confocal images of the drug loaded SF spheres are shown in Fig. 5, and the drug loading and distribution in SF spheres can be observed. Silk spheres displaying distinct encapsulation efficiencies of drug molecules were mainly due to the different interactions between the drug molecules and carriers. For instance, RhB as a hydrophobic molecule with positive charge and low MW can easily diffuse in the SF spheres, and the electrostatic interactions between the molecule and SF could stabilize the RhB in the carrier with the enhanced encapsulation efficiency.

In case of SF spheres with different MW, the SF spheres pre-

Table 3. Drug loading efficiency of SF spheres prepared from different MW of RSF

	Property	Sample	Initial loading (μg/mg silk)	Loading efficiency (%)	Actual loading (μg/mg SF spheres)
FITC-BSA	Hydrophobic Negative charge Log P: 0.1-0.5 66 kDa	30 min (290 kDa) 45 min (190 kDa) 60 min (120 kDa)	5	35.56 28.65 25.87	2.517 1.555 1.399
FITC-Dex	Hydrophilic Neutral Log P: −7.2 10 kDa	30 min (290 kDa) 45 min (190 kDa) 60 min (120 kDa)	5	2.38 3.78 4.48	0.167 0.197 0.240
RhB	Hydrophobic Positive charge Log P: 1.95 479 Da	30 min (290 kDa) 45 min (190 kDa) 60 min (120 kDa)	5	44.39 74.58 68.88	3.508 4.315 3.915

Note: Log P: lower value indicates hydrophilic, while a higher value indicates hydrophobic.

pared from high MW of RSF could load more macromolecular drug with negative charge compared to middle and low MW RSF. However, the SF spheres prepared from low MW of RSF could present a high encapsulation efficiency for the positive charge and low MW drug. Furthermore, it was straightforward to observe the distribution of drug molecule by confocal scanning microscopy. FITC-BSA loaded SF spheres showed green fluorescence, indicating the distribution of molecule in SF spheres and displayed different intensity of fluorescence according to the amount of molecule in the spheres. For the FITC-Dex, the green florescence was very weak, indicating few Dex were encapsulated in the silk spheres, which was consistent with the data in Table 3. RhB loaded SF spheres emitted strong red fluorescence with a molecule distribution on the periphery of the spheres rather than the center.

Afterwards, the drug release profiles were explored (Fig. 6). In the first 8 h, a burst release was presented in every drug-loaded SF sphere, probably due to the drug release from the amorphous region or near the surface of SF spheres which was easy to swell in PBS buffer solution with a short diffusion distance. In the case of FITC-BSA, the amount of cumulative release is basically opposite to the amount of loading, and less than 23% of total encapsulation was released within ten days from the low MW SF spheres (Fig. 6(a)), only about 6% of drug was released from high MW SF spheres. FITC-Dex released much faster with more than 97% of total loading drug released within 48 h (Fig. 6(b)). Because, the loading efficiency is low and molecule could not be stabilized in the SF spheres. As a low molecular weight, positive charge and hydrophobic model, RhB was released from SF based carrier with a slow-release rate, the rule of which is similar to the case of BSA, but the release efficiency is better than BSA. Under the same initial amount, SF based carrier from 45 min (190 kDa) sample showed a high loading and relative slow-release rate, which might be ascribed to the adaptability of the drug molecule and carrier including molecule property, structure of SF spheres, such as β-sheet content of SF, the size of carrier and the drug-loading capacity of carrier (Fig. 6(c)).

To explore the release mechanisms in-depth, the release kinetics was examined by evaluating the different kinetics models for the drug-loaded SF spheres. Table 4 displays the simulated in vitro release parameters applying different kinetics models as zero-order, first-order and Korsmeyer-Peppas [58]. According to the coefficient of determination, all data fitted well with Korsmeyer-Peppas model compared to others (Table 4). The release exponents of all the cases in this work were calculated to be less than 0.43 (Table 4), which implied that the release kinetics of drug loaded SF spheres

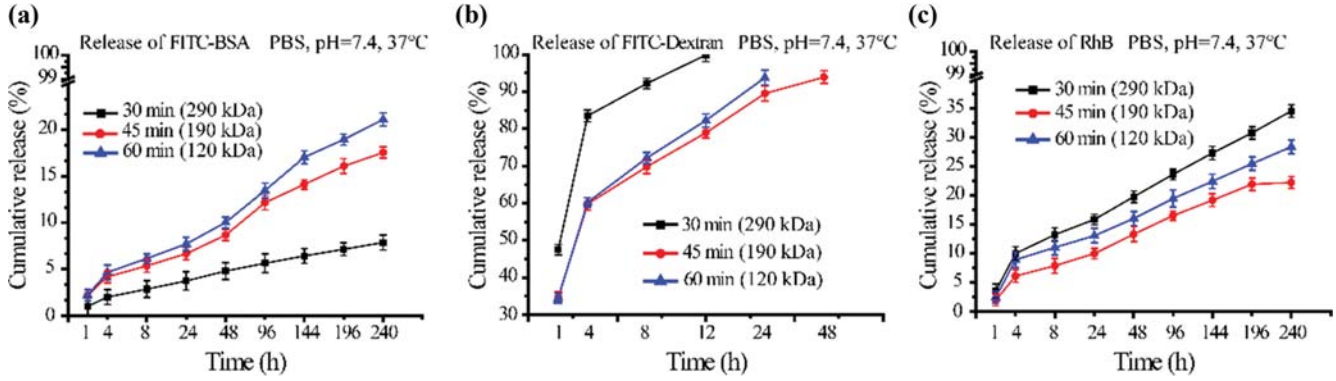

Fig. 6. Cumulative drug release from drug-loaded SF spheres. (a) FITC-BSA release, (b) FITC-Dextran release, (c) RhB release from SF spheres prepared by different MW. The black, red and blue curves represent the drug release of SF spheres prepared from three MW of RSF, respectively. To determine drug release, the SF spheres were spun down at certain time points and drug concentrations in the supernatants were measured. The vertical coordinate was percentage of cumulative drug release amount to actual loading amount at the corresponding time points.

Table 4. Release Kinetics of FITC-BSA, FITC-Dextran and RhB loaded SF spheres fitting with different models

Sample		Drug release kinetics (R^2)			Release exponent (n) in Korsmeyer-Peppas
		Zero-order	First-order	Korsmeyer-Peppas	
FITC-BSA	30 min (290 kDa)	0.8803	0.8866	0.9929	0.322
	45 min (190 kDa)	0.9406	0.9504	0.9926	0.383
	60 min (120 kDa)	0.9485	0.9598	0.9905	0.406
FITC-Dex	30 min (290 kDa)	0.8048	0.8843	0.9221	0.273
	45 min (190 kDa)	0.6477	0.8993	0.9207	0.221
	60 min (120 kDa)	0.8035	0.8611	0.9712	0.288
RhB	30 min (290 kDa)	0.8902	0.9220	0.9807	0.319
	45 min (190 kDa)	0.8774	0.8964	0.9884	0.344
	60 min (120 kDa)	0.8834	0.9109	0.9727	0.317

Table 5. STM loading efficiency of SF spheres prepared from different MW of RSF

	Property	Sample	Initial loading (μg/mg silk)	Loading efficiency (%)	Actual loading (μg/mg SF spheres)
STM	Hydrophilic Positive charge Log P: −6.4 581 Da	30 min (290 kDa) 45 min (190 kDa) 60 min (120 kDa)	5	60.5 73.3 64.7	3.63 4.54 4.02

conform to Fickian diffusion [46,59], especially for the case of RhB-loaded SF spheres.

5. Antibacterial Activity Test with Controlled Release

We systematically investigated the effect of molecular weight on SF spheres for drug delivery, and the specificity of drug carrier according to the different drug molecule was examined, which could be applied in the killing bacteria with controlled release that is a useful way and also comparable to other antimicrobial strategies [60-63]. Streptomycin is an aminoglycoside antibiotic that has been widely used in human disease therapy, for instance, as a veterinary medicine to against bacterial infections, such as Mycobacterium tuberculosis [64]. However, it has a narrow therapeutic range and too much dosage could lead to serious side effects such as nephro and ototoxicity [65,66]. Therefore, the dosage control and efficient drug delivery system are required for STM utilization. We proposed a strategy based drug-loading SF spheres to monitor and assess the control release of STM against the *E. coli* as the model bacteria. STM is a low MW molecule with positive charge, and the feature is similar to RhB. Therefore, SF spheres loaded and released RhB could be applied in this case.

Initially, as shown in Table 5, encapsulation efficiency of STM-loaded SF spheres prepared from different MW of SF (following the above procedure) were calculated to be 60.5% for 30 min (290 kDa) sample, 73.3% for 45 min (190 kDa) sample and 64.7% for 60 min (120 kDa) sample. Thus, the SF spheres prepared from 45 min (190 kDa) with relatively highest loading efficiency were used in sustained release antibacterial experiment, and the actual loading amount of STM was 110 μg for SF spheres prepared from 45 min (190 kDa) in this case. The bacteria *E. coli* (10 μL, 2×10^7 cfu/mL) could not be inhibited and killed without any treatment (Fig. 7(a)) or just treated by SF spheres without STM drug. Low dosage of STM (10 μg/mL, more than MBC of STM) could kill the bacteria in the first 12 hours, but failed to disinfect it in 24 hours, which could be due to excessive consumption of STM besides the

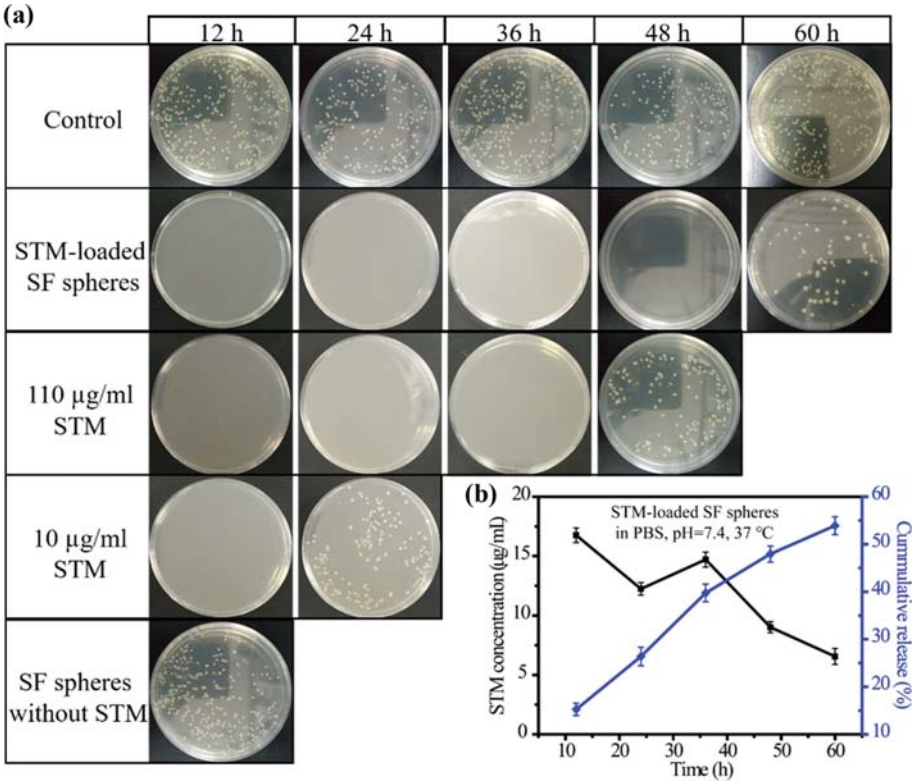

Fig. 7. Antimicrobial activity of STM and STM loaded SF spheres. (a) Images of bacterial colonies of *E. coli* treated by STM (110 μg/mL, 10 μg/mL), STM loaded SF spheres, SF spheres and PBS. (b) The cumulative release of STM from SF spheres, the release medium and conditions of STM loaded SF spheres were PBS, pH=7.4 and 37 °C, respectively.

Table 6. Release Kinetics of STM loaded SF spheres fitting with different models

Sample		Drug release kinetics (R^2)			Release exponent (n) in Korsmeyer-Peppas
		Zero-order	First-order	Korsmeyer-Peppas	
STM	45 min (190 kDa)	0.9895	0.9985	0.9853	0.76

MBC. Although we increased the dosage of STM to 110 μg/mL, it could maintain the antimicrobial activity for 36 hours. However, the disadvantage of the high dosage of antibiotic used could induce the drug-resistance of bacteria and the other side effect. The STM-loading SF spheres presented the slow-release and 48 hours long-term sterilization, which exhibits an advantage compared to the bared streptomycin. The dosage of STM via the control release was explored based on the SF carrier (Fig. 7(b)). The concentration of STM released from the carrier and the accumulative amount vs. time was examined and more than 10 μg/mL STM could be detected from carrier, and the accumulative amount increased up to 55% of loading drug after 60 hours. The SF based sphere proved to be a good drug carrier for the loading and release of STM, considering the adaptability between the drug and the drug carrier. The control release of STM in the SF based carrier maintains the bioactivity and stability of the drug molecule, and also prolongs the time of sterilization and avoids the excessive consumption of streptomycin.

Table 6 displays the simulated in vitro release parameters applying different kinetics models as zero-order, first-order and Korsmeyer-Peppas. It was found that the release kinetic fitted well with first-order model compared to others. The release kinetics of STM was different from that of rhodamine, possibly because the log P of STM is much lower than that of RhB, which might lead to the fact that the hydrophobicity of STM was lower than RhB. For the Korsmeyer-Peppas model, the value of n was 0.76; it could be suggested that the mechanism that led to the release of STM was an anomalous non-Fickian diffusion transport, which indicated that the drug release occurred through diffusion in the SF spheres matrix and polymer relaxation [67].

CONCLUSIONS

We constructed different SF carriers by regulating the MW distribution and examined the loading and release of drugs with distinct properties, (*e.g.*, MW and charge) considering the adaptability between the drug and drug spheres. The SF based spheres prepared from high MW of RSF could load more macromolecular drug with negative charge but normal releasing compared to middle and low MW RSF. While, the drug carrier prepared from low MW of RSF could present a high encapsulation efficiency and rational releasing for the positive charge and low MW drug, compared to other spheres. Finally, the SF based drug spheres were used to encapsulate antibiotic streptomycin for sterilization with long-term and controlled-release, and it presented a good advantage compared to bared streptomycin in solution. This work provides a guideline for the choice of transport vehicle for more effective drug delivery and a utilization through a simple, rapid, applicable and low-cost method, and it might also be useful for SF based drug delivery systems.

ACKNOWLEDGEMENT

The authors gratefully acknowledge the financial support from National Natural Science Foundation (21573097, 51503087).

NOTES

The authors declare no competing financial interest.

NOMENCLATURE

Symbols

C : concentration
°C : degree centigrade
h : hour
mg : milligram
μg : microgramme
mL : milliliter
mmoL : millimole
moL : moore

Abbreviations

FITC-BSA : fluorescein isothiocyanate conjugated bovine serum albumin
FITC-Dextran : fluorescein isothiocyanate conjugated dextran
MW : molecular weight
PVA : polyvinyl alcohol
RSF : regenerated silk fibroin
SEM : scanning electron microscopy
SF : silk fibroin
STM : streptomycin

REFERENCES

1. D. Rockwood, R. Preda, T. Yücel, X. Wang, M. Lovett and D. Kaplan, *Nat. Protoc.*, **6**, 1612 (2011).
2. M. Farokhi, F. Mottaghitalab, R. L. Reis, S. Ramakrishna and S. C. Kundu, *J. Control. Release*, **321**, 324 (2020).
3. X. Wang, T. Yucel, Q. Lu, X. Hu and D. L. Kaplan, *Biomaterials*, **31**, 1025 (2010).
4. Y. Liu, L. Huang, W. Yuan, D. Zhang, Y. Gu, J. Huang and S. Murphy, *J. Biomed. Mater. Res. Part A*, **108**, 1760 (2020).
5. Z. Ding, Z. Fan, X. Huang, Q. Lu, W. Xu and D. L. Kaplan, *ACS Appl. Mater. Interfaces*, **8**, 24463 (2016).
6. Q. Zhang, H. Yu, M. Barbiero, B. Wang and M. Gu, *Light: Science & Applications*, **8**, 42 (2019).
7. J.-P. Jiang, X.-Y. Liu, F. Zhao, X. Zhu, X.-Y. Li, X.-G. Niu and Z.-T.

Yao, *Neural Regen. Res.*, **15**, 1961 (2020).
8. Y. Y. Han, S. H. Yu, L. C. Liu, S. J. Zhao, T. X. Yang, Y. J. Yang, Y. M. Fang and S. S. Lv, *Mol. Catal.*, **457**, 24 (2018).
9. Y. Srisuwan, P. Srihanam and Y. Baimark, *J. Macromol. Sci. Part A-Pure Appl. Chem.*, **46**, 521 (2009).
10. L. Liu, K. Busuttil, S. Zhang, Y. L. Yang, C. Wang, F. Besenbacher and M. D. Dong, *PCCP*, **13**, 17435 (2011).
11. L. Liu, L. H. Klausen and M. Dong, *Nano Today*, **23**, 40 (2018).
12. L. Liu, X. Tian, Y. Ma, Y. Duan, X. Zhao and G. Pan, *Angew. Chem. Int. Ed.*, **57**, 7878 (2018).
13. L. Liu, Y. Li, D. Xia, C. Bortolini, S. Zhang, Y. Yang, J. S. Pedersen, C. Wang, F. Besenbacher and M. Dong, *Nanoscale*, **7**, 2250 (2015).
14. C. Vepari and D. L. Kaplan, *Prog. Polym. Sci.*, **32**, 991 (2007).
15. K.-J. Kwon and H. Seok, *Appl. Sci.*, **8**, 1214 (2018).
16. S. Kapoor and S. C. Kundu, *Acta Biomater.*, **31**, 17 (2016).
17. D. T. Pham, N. Saelim and W. Tiyaboonchai, *Drug Deliv. Transl. Res.*, **10**, 1 (2019).
18. J. Wu, J. Wang, J. Zhang, Z. Zheng, D. L. Kaplan, G. Li and X. Wang, *ACS Biomater. Sci. Eng.*, **4**, 3885 (2018).
19. P. Shi and J. C. H. Goh, *Int. J. Pharm.*, **420**, 282 (2011).
20. J. Wu, Z. Zheng, G. Li, D. L. Kaplan and X. Wang, *Acta Biomater.*, **39**, 156 (2016).
21. A. N. Mitropoulos, G. Perotto, S. Kim, B. Marelli, D. L. Kaplan and F. G. Omenetto, *Adv. Mater.*, **26**, 1105 (2014).
22. J. A. Champion, Y. K. Katare and S. Mitragotri, *J. Control. Release*, **121**, 3 (2007).
23. C. Michaela, S. Apoorva, H. Masoud, D. A. Fedosov, M. Samir and S. G. Anirban, *Nanoscale*, **10**, 15350 (2018).
24. H. T. Ta, N. P. Truong, A. K. Whittaker, T. P. Davis and K. Peter, *Expert Opin. Drug Deliv.*, **15**, 33 (2018).
25. M. Mehrabadi, D. N. Ku and C. K. Aidun, *Phys. Rev. E*, **93**, 023109 (2016).
26. P. H. M. Hoet, I. Brüske-Hohlfeld and O. V. Salata, *J. Nanobiotechnol.*, **2**, 12 (2004).
27. R. C. Mundargi, V. R. Babu, V. Rangaswamy, P. Patel and T. M. Aminabhavi, *J. Control. Release*, **125**, 193 (2008).
28. A. P. Tabatabai, B. P. Partlow, N. R. Raia, D. L. Kaplan and D. L. Blair, *Langmuir*, **34**, 15383 (2018).
29. H. H. Kim, D. W. Song, M. J. Kim, S. J. Ryu, I. C. Um, C. S. Ki and Y. H. Park, *Polymer*, **90**, 26 (2016).
30. L. S. Wray, X. Hu, J. Gallego, I. Georgakoudi, F. G. Omenetto, D. Schmidt and D. L. Kaplan, *J. Biomed. Mater. Res. B Appl. Biomater.*, **99B**, 89 (2011).
31. J. B. Wu, Z. Z. Zheng, G. Li, D. L. Kaplan and X. Q. Wang, *Acta Biomater.*, **39**, 156 (2016).
32. J. Wang, S. Zhang, T. Xing, B. Kundu, M. Li, S. C. Kundu and S. Lu, *Int. J. Biol. Macromol.*, **79**, 316 (2015).
33. J. Wang, Z. Yin, X. Xiang, S. C. Kundu, X. Mo and S. Lu, *Int. J. Mol. Sci.*, **17**, 2012 (2016).
34. O. Cheerarot and Y. Baimark, *E-Polymers*, **15**, 67 (2015).
35. S. Y. Kim, D. Naskar, S. C. Kundu, D. P. Bishop, P. A. Doble, A. V. Boddy, H. K. Chan, I. B. Wall and W. Chrzanowski, *Sci. Rep.*, **5**, 11878 (2015).
36. D. N. Breslauer, S. J. Muller and L. P. Lee, *Biomacromolecules*, **11**, 643 (2010).
37. A. S. Lammel, X. Hu, S.-H. Park, D. L. Kaplan and T. R. Scheibel, *Biomaterials*, **31**, 4583 (2010).
38. E. Wenk, A. Wandrey, H. Merkle and L. Meinel, *J. Control. Release*, **132**, 26 (2008).
39. D. T. Pham, N. Saelim and W. Tiyaboonchai, *Colloids Surf. B: Biointerfaces*, **181**, 705 (2019).
40. D. T. Pham and W. Tiyaboonchai, *Drug Deliv.*, **27**, 431 (2020).
41. M.-H. Alves, B. E. B. Jensen, A. a. A. Smith and A. N. Zelikin, *Macromol. Biosci.*, **11**, 1293 (2011).
42. M. I. Baker, S. P. Walsh, Z. Schwartz and B. D. Boyan, *J. Biomed. Mater. Res. B Appl. Biomater.*, **100B**, 1451 (2012).
43. P. J. Shi and J. C. H. Goh, *Powder Technol.*, **215-216**, 85 (2012).
44. Y. Baimark, P. Srihanam, Y. Srisuwan and P. Phinyocheep, *J. Appl. Polym. Sci.*, **118**, 1127 (2010).
45. M. Chen, Z. Shao and X. Chen, *J. Biomed. Mater. Res. Part A*, **100A**, 203 (2012).
46. D. Y. Arifin, L. Y. Lee and C.-H. Wang, *Adv. Drug Deliv. Rev.*, **58**, 1274 (2006).
47. Y. J. Li, S. University, F. Q. Supervision, T. Center and M. O. Agriculture, *Food Industry*, **357**, 1565 (2008).
48. T. Tanaka, M. Suzuki, N. Kuranuki, T. Tanigami and K. Yamaura, *Polym. Int.*, **42**, 107 (1997).
49. T. Tanaka, T. Tanigami and K. Yamaura, *Polym. Int.*, **45**, 175 (1998).
50. X. Chen, Z. Shao, N. S. Marinkovic, L. M. Miller, P. Zhou and M. R. Chance, *Biophys. Chem.*, **89**, 25 (2001).
51. M. Sonoyama and T. Nakano, *Appl. Spectrosc.*, **54**, 968 (2016).
52. X. Hu, D. Kaplan and P. Cebe, *Macromolecules*, **39**, 6161 (2006).
53. M. Kaszuba, J. Corbett, F. M. Watson and A. Jones, *Philos. Trans. R. Soc. A-Math. Phys. Eng. Sci.*, **368**, 4439 (2010).
54. J. Panyam, D. Williams, A. Dash, D. Leslie-Pelecky and V. Labhasetwar, *J. Pharm. Sci.*, **93**, 1804 (2004).
55. S. B. Sawant, J. B. Joshi and S. K. Sikdar, *Biotechnol. Tech.*, **2**, 41 (1988).
56. U. Gunduz, *Bioseparation*, **9**, 277 (2000).
57. H. Yoshimizu and T. Asakura, *J. Appl. Polym. Sci.*, **40**, 1745 (1990).
58. J. Siepmann and N. A. Peppas, *Adv. Drug Deliv. Rev.*, **48**, 139 (2001).
59. J. Siepmann and F. Siepmann, *Int. J. Pharm.*, **364**, 328 (2008).
60. J. Zhang, Y. Feng, J. Mi, Y. Shen, Z. Tu and L. Liu, *J. Hazard. Mater.*, **342**, 121 (2018).
61. Q. Chen, L. Zhang, Y. Feng, F. Shi, Y. Wang, P. Wang and L. Liu, *J. Mat. Chem. B*, **6**, 7643 (2018).
62. Y. Feng, L. Liu, J. Zhang, H. Aslan and M. Dong, *J. Mat. Chem. B*, **5**, 8631 (2017).
63. Y. Feng, Q. Chen, Q. Yin, G. Pan, Z. Tu and L. Liu, *ACS Appl. Bio Mater.*, **2**, 747 (2019).
64. E. T. Mcenery, H. C. Sweany and G. C. Turner, *Ill. Med. J.*, **4**, 15 (1950).
65. M. A. Omar, M. A. Hammad, D. M. Nagy and A. A. Aly, *Spectrochim. Acta Part A: Mol. Biomol. Spectrosc.*, **136**, 1760 (2015).
66. T. A. Savidge, *Biotechnology of industrial antibiotics*, Vanvdamme, E. J. (ed.), Marcel Dekker Inc., New York (1984).
67. L. Nori, S. S. ManiKiran and N. Rao, *Int. J. PharmTech Res.*, **2**, 2506 (2010).